Hindawi
Advances in Civil Engineering
Volume 2018, Article ID 1465672, 17 pages
https://doi.org/10.1155/2018/1465672

Research Article

A New Mining Scheme for Hanging-Wall Ore-Body during the Transition from Open Pit to Underground Mining: A Numerical Study

Baohui Tan,[1] **Fengyu Ren**,[1] **Youjun Ning**,[2,3,4] **Rongxing He**,[1] **and Qiang Zhu**[5]

[1]*School of Resources and Civil Engineering, Northeastern University, Shenyang 110819, China*
[2]*School of Manufacturing Science and Engineering, Southwest University of Science and Technology, Mianyang 621010, China*
[3]*State Key Laboratory of Coal Resources and Safe Mining, China University of Mining and Technology, Xuzhou 100083, China*
[4]*Shock and Vibration of Engineering Materials and Structures Key Laboratory of Sichuan Province, Southwest University of Science and Technology, Mianyang 621010, China*
[5]*School of Environment and Resource, Southwest University of Science and Technology, Mianyang 621010, China*

Correspondence should be addressed to Youjun Ning; cnningyj@foxmail.com

Received 17 July 2018; Accepted 12 September 2018; Published 17 October 2018

Guest Editor: Dengke Wang

A new mining scheme by employing the induced caving mining method to exploit hanging-wall ore-body during the transition from open pit to underground mining is proposed. The basic idea is to use the mined-out area generated by the planned mining of the hanging-wall ore-body to absorb the collapsed slope body, so as to avoid the influence of the inner-slope mining to the normal open-pit mining and guarantee mining efficiency during the transition stage. Numerical simulation study on the process of induced caving mining of hanging-wall ore-body is carried out based on the practical engineering setting of the Hainan iron mine, China, by employing the numerical method of discontinuous deformation analysis (DDA). The impact of rock mass structure on the mechanism of slope instability development and the mining hazard assessment in the new mining scheme is investigated. The influence of mining sequence on slope instability development and mining safety is also analyzed by taking the hanging-wall ore-body mining under the southern anti-dip slope at the Hainan iron mine as an example, and eventually a reliable mining scheme via induced caving is obtained. The numerical study proves the feasibility of the proposed new mining scheme for hanging-wall ore-body and provides theoretical and technical support for its application in practical mining activities.

1. Introduction

The hanging-wall ore-body is the ore-body which residues inside open-pit slope after the normal surface mining. Figure 1 shows a mode of the occurrence of hanging-wall ore-body at the Dagushan Iron Mine in China. According to statistical data, the residual ore-body outside the open-pit boundary accounts for 5–16% or even more of the total reserve until the open pit is closed [1].

In order to exploit sufficiently mineral resource and realize the smooth transition for the ore output, it is necessary to extract the hanging-wall ore-body during the transition from open pit to underground mining. However, it is highly challenging to operate simultaneously normal open-pit mining and mining for hanging-wall ore-body. Traditional mining methods for hanging-wall ore-body include surface mining and back-fill stoping method such as that in the Fenghuangshan Iron Mine of China and the Kidd Creek Zinc-copper Mine of Canada, the sublevel caving method such as that in the Yeshan Iron Mine and the Longshou Mine of China, and the sublevel open stoping and caving mining method such as that used by Liu et al. [1]. Unfortunately, all these mining methods cannot terminate the serious mutual restriction between the hanging-wall ore-body mining and the normal open-pit mining during the transition stage. For instance, when using the open stoping and back-fill stoping method to extract hanging-wall ore-body, it is needed to limit the stope scale or adopt additional

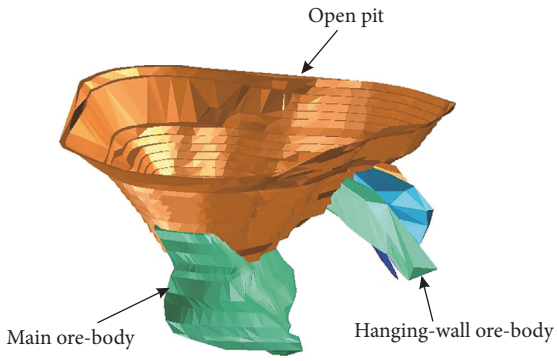

Figure 1: A mode of the occurrence of hanging-wall ore-body at the Dagushan Iron Mine in China.

reinforcement of the open-pit slope, so that the mining efficiency is restricted; a large scale of slope instability could occur at the initial stage of mining when using the sublevel caving method to extract hanging-wall ore-body [2]; therefore, it has to limit the starting time of hanging-wall ore-body mining to ensure the safety of open-pit operation. Generally, these traditional mining methods fail to achieve large-scale mining of hanging-wall ore-body during the transition stage, which causes ore output decline for most mines in this period. Although there are a lot of studies on opencast-underground combined mining [3–5], it is rarely mentioned how to realize simultaneously the effective and safe operation of the open-pit mining and inner-slope mining during the transition stage.

In traditional mining methods, the slope usually needs to be stable when open-pit mining and inner-slope mining are operated simultaneously, which limits the stope scale and restricts the mining efficiency of the hanging-wall ore-body. In the present study, a new mining scheme for hanging-wall ore-body during the transition stage by employing a newly improved underground mining method, namely, the induced caving mining method, is proposed. In this scheme, the slope is allowed to collapse to a certain degree and the collapsed slope body is supposed to be absorbed by the mined-out area generated by the planned mining of the hanging-wall ore-body. This mining scheme could avoid the influence of the inner-slope mining to the normal open-pit mining and thus guarantee the mining efficiency during the transition stage. Apparently, the slope instability behavior, which is greatly controlled by the rock mass structure of the slope and the exact mining plan (e.g., mining sequence), has a significant impact on the application of the proposed mining scheme. Therefore, numerical simulations will be carried out to investigate this problem in the present study.

Numerical modeling is an important modern research approach, and it is expected to reproduce the displacement, stress, and strain distribution pattern of rock mass during mining thorough numerical simulations. Continuum-based numerical simulation methods, such as the finite difference method (FDM) and the finite element method (FEM), were widely applied to study the patterns of the movement and failure of the strata and surface induced by underground mining. For example, Zhao et al. [6] used the FDM software FLAC^{3D} to obtain the responding laws of the deflection and horizontal thrust of the roof rock beam under shallow mining conditions. Lin et al. [7] used the FLAC^{3D} to analyze the surface response and interaction of two layers of superthick coal seam mining. Li et al. [8] used the FLAC^{3D} to determine the minimum thickness of the safe mining roof of submarine gold deposits. Meanwhile, the FEM method was applied to assess the stability of debris and rock slopes [9], to determine the elastic compliance tensor of fractured rock masses [10], and to simulate rock cutting and its fragmentation process [11]. It has certain defects to regard the rock mass as a continuous material when using the FDM and FEM to simulate mining problems. Discontinuous deformation and movement and large displacement are greatly involved in the surrounding rock for underground mining and in the slope rock for open-pit mining when slope failure takes place.

On the other hand, discontinuum-based numerical methods, such as the discrete element method (DEM) [12] and the discontinuous deformation analysis (DDA) [13] method, are by nature capable of simulating discontinuous and large displacement of rock masses. For example, the DEM-based software UDEC has been used to simulate the slope instability caused by the hanging-wall ore-body mining with the sublevel caving method [2]. The DEM-based software PFC^{3D} has been used to analyze the failure process of soil-rock mixtures [14]. The DDA has been used to simulate the excavation of the tunnel and its reinforcement in columnar jointed basalt [15]. In addition, some researchers used discrete element and finite element coupling methods to simulate large-scale underground excavation [16, 17]. Another unified continuous-discontinuous numerical method, namely, the numerical manifold method (NMM), has been used to analyze the stability and failure characteristics of the footwall slope [18].

In the present study, the DDA is adopted as the numerical method to do numerical simulations of the discontinuous deformation/movement and large displacement of the open-pit slope caused by inner-slope mining with the proposed mining scheme of hanging-wall ore-body. Key factors affecting the implementation of the mining scheme, such as the rock mass structure and the mining sequence, are deeply investigated through DDA simulations of instances based on practical engineering settings. The proposed mining scheme is proved to be feasible, and some theoretical and technical guidance for the application of the mining scheme in practical mining operation are provided.

2. New Mining Scheme for Hanging-Wall Ore-Body via the Induced Caving Mining Method

2.1. Induced Caving Mining Method. The so-called induced caving mining method is a newly improved underground mining method as a combination of the block caving mining method (Figure 2(a)) and the sublevel caving mining method (Figure 2(b)) essentially. It contains the ore-body breakage process by underground pressure in block caving, and the drilling, blasting, and drawing process in sublevel caving. Figure 3 shows a typical induced caving mine layout.

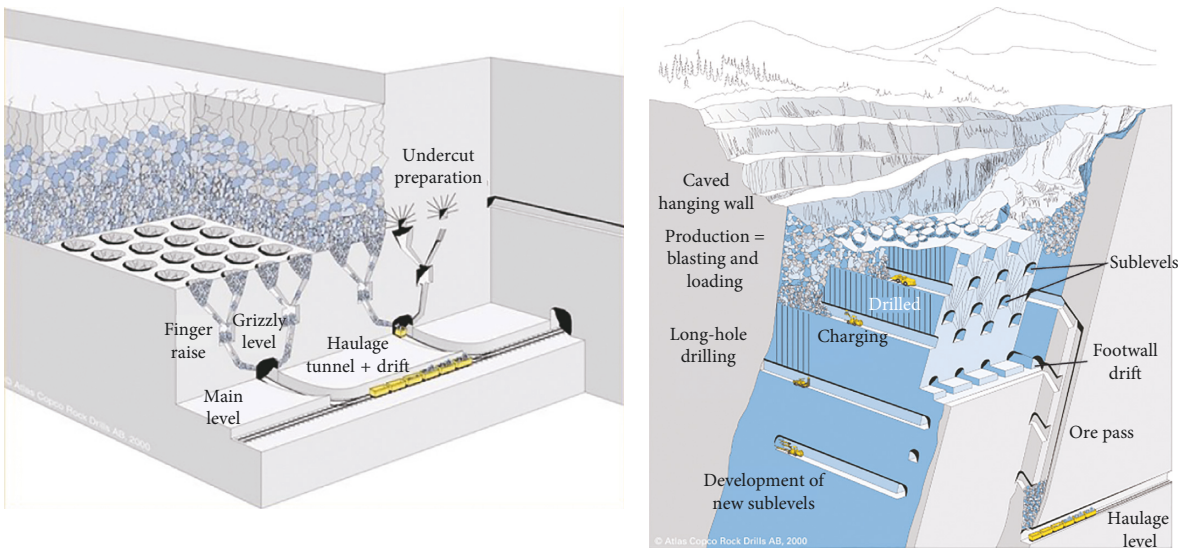

(a) (b)

Figure 2: Illustration of typical (a) block caving mining and (b) sublevel caving mining operations (image copyright: Atlas Copco).

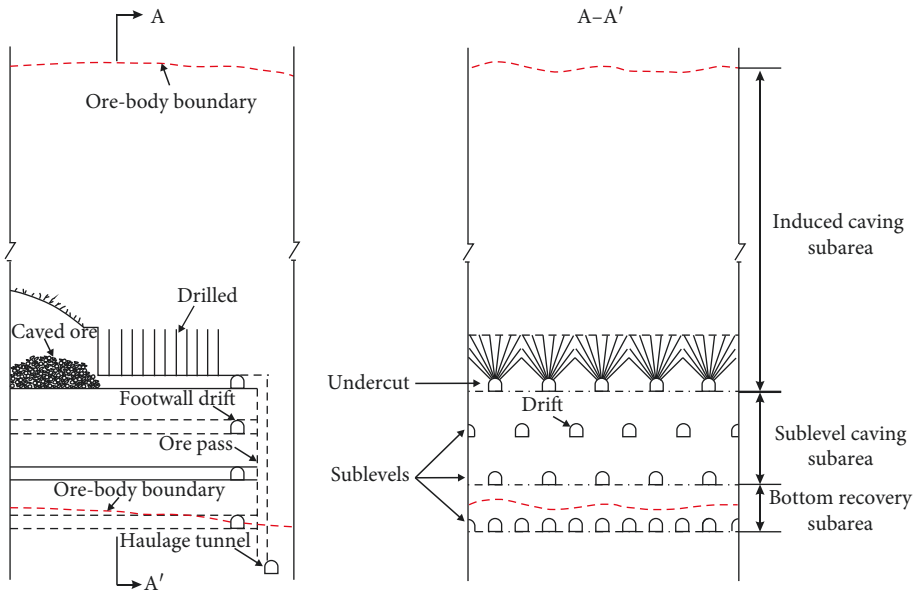

(a) (b)

Figure 3: A typical induced caving mine layout.

The ore-body is partitioned vertically downwards into three subareas with different mining characteristics, called the induced caving subarea, the sublevel caving subarea, and the bottom recovery subarea, respectively.

The mining layer placed in the bottom of the induced caving subarea is regarded as the undercut level, and an extensive horizontal panel (undercut) beneath the mined block is formed by fan-shaped hole blasting. It should be noted that in the undercutting process, only about 30–50% of the volume of the blasted ore is extracted after each blasting, so as to provide a swell volume for the roof caving, while the remaining blasted ore temporarily stays at the undercut as a buffer layer to prevent the impact harm during the roof caving. Stress redistribution and gravity combine to trigger the roof progressive fracturing and caving into the undercut, and the caved ore is extracted in the mining process of sublevels below. Fracturing and caving extend progressively upwards as the caved ore is extracted, resulting in significant surface depression. In the sublevel caving subarea, usually at least two sublevels are placed to make sure a sufficient extraction of the caved ore above. The mining operation in the sublevel caving subarea is exactly

the same as that in the sublevel caving mining method. The bottom recovery subarea provides the last chance for recovering the ore in the stope. Therefore, dense production drifts in this mining subarea are employed to improve the ore recovery rate. It can be seen that the induced caving combines the advantages of large capacity, low cost of the block caving, and simple layout, flexible application of the sublevel caving. At present, the induced caving mining method is being applied to several mines in China, such as the Xiaowanggou Iron Mine, the Yanqianshan Iron Mine, the Beiminghe Iron Mine, and the Paishanlou Gold Mine, etc.

2.2. The Induced Caving Mining of Hanging-Wall Ore-Body. Successful application cases of the induced caving mining method improve the understanding of the mechanism of roof caving and surface subsidence. On this basis, a new mining scheme for hanging-wall ore-body via induced caving during the transition from open pit to underground mining, as illustrated in Figure 4, is proposed to avoid the influence of inner-slope mining on the normal open-pit mining and balance the risks and benefits of hanging-wall ore-body mining in the transition stage.

Due to the effects of weathering, surface blasting vibration, and mining unloading, etc., the hanging-wall ore-body usually becomes favorable to be caved. Based on the preexisting development engineering of the open pit, it is convenient to implement the underground operation of the hanging-wall ore-body mining. As shown in Figure 4, an undercut level is placed within the ore-body to induce the upper ore to cave. While caving extends progressively upwards as the broken ore is extracted gradually, the slope will collapse when the caving reaches to a certain degree. It is expected that with a rational mining strategy, mainly including the design of mining span, height, and sequence, the occurrence time and the scale of the slope instability can be controlled, ensuring that there is enough mined-out area to absorb the collapsed slope body when the slope instability occurs. In such a way, the threat of slope instability to the normal open-pit mining can be eliminated, and the influence of the hanging-wall ore-body mining on the open-pit mining can be avoided. With perfect implementation, the proposed mining scheme can protect the normal open-pit mining from the threat of the slope instability throughout the whole transition stage. Moreover, some monitoring techniques, such as GB-InSAR, LiDAR, etc, can be used to forecast the slope instability to improve the safety of this mining scheme. In terms of mining strategy planning, both the block caving and sublevel caving can provide a lot of practical experiences [19, 20]. In the following, DDA simulations based on practical engineering settings will be carried out to examine the feasibility of the proposed mining scheme and the key influencing factors.

3. Engineering Background of Numerical Investigation

The Hainan Iron Mine is an open-pit mine located in Changjiang Li Autonomous County, Hainan, China. It is a large sedimentary metamorphic iron deposit. The ore-body is chiefly composed of hematite and its surrounding rock mainly consists of dolomite, phyllite, and quartz-schist. The main ore-body situates at an elevation of −601.91 m to 202.44 m, with a length of 1670 m east-west, and a horizontal projection width of 350 m. The open pit with the closed loop at 168 m is being developed at an elevation of 24 m, and as planned, it will turn into underground mining below an elevation of 0 m. The south and north slopes of the open pit have hanging-wall ore-bodies below, which are primarily branches of the main ore-body and also individuals around. According to a series of geological surveys, the rock mass in the slope of the open pit mainly consists of two joint sets with good persistence. One set is approximately horizontal with evenly spaced bedding planes with a dip angle varying slightly with the survey sites (basically maintained within 0°~5°) and the interlayer spacing is approximately 1.0 m, whereas the other set points to the foot of the north slope and inwards to the south slope with the dip angle and interlayer spacing varying significantly. The two main joint sets intersect to cut the rock into a jointed rock mass. Figure 5 shows the distribution of the geological survey sites and the sectional views of the south and north slopes.

The induced caving mining will be considered for the hanging-wall ore-bodies in the south and north slopes in Figure 5. According to the joint set orientations and some literatures of slope instability studies [21, 22], due to the mining of the hanging-wall ore-bodies via induced caving, the north slope may take place sliding failure, whereas the south slope may take place topping failure. Determining slope instability under various mining conditions and the internal mechanisms and controlling factors is obviously impossible merely on a visual and empirical basis. In the next two sections, DDA simulation study on induced caving mining of the hanging-wall ore-bodies will be conducted, and two major factors, namely, the rock structure and the mining sequence will be considered.

4. Effect of Rock Mass Structure

4.1. Model Establishment and Simulation Scenarios. Based on the engineering background of Hainan iron mine, six numerical simulation instances are carried out to evaluate the significance of rock mass structure in the development of the slope instability and mining hazard assessment.

In the six simulation models constructed, the slope rock mass all contains two joint sets, marked as j_1 and j_2, respectively. The dip angle of j_1 maintains 0° consistently, representing the approximate horizontal bedding plane in practice. The dip angle of j_2 is changed from 50° to 150°, and the value is taken every 20°, representing the other major joint set with the dip angle varying with the survey sites. When the dip angles of the j_2 are 50°, 70°, and 90°, the j_2 points to the toe of slope, corresponding to the north slope, while the j_2 are inclined at 110°, 130°, and 150°, the j_2 points inwards the slope, corresponding to the south slope. Figure 6 shows the geometry of the model and locations of the measurement points in the simulation. In addition, modeling according to the actual joint spacing will result in

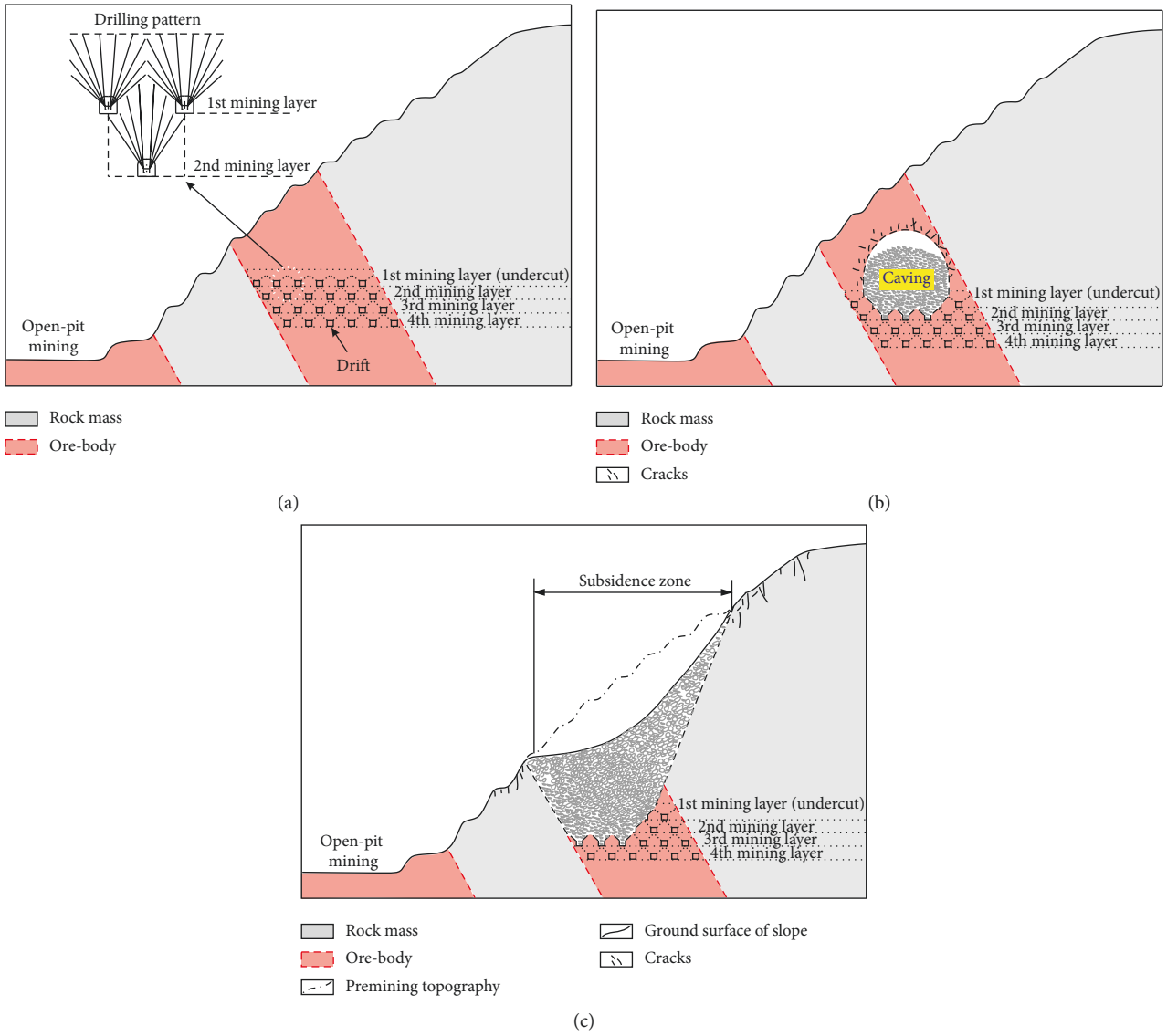

FIGURE 4: Illustration of mining scheme for hanging-wall ore-body via the induced caving mining method. (a) Mine layout. (b) Caving after undercutting. (c) Slope failure due to mining.

excessive calculation due to the large number of rock blocks in the model. To reduce the calculation amount, the spacing of both joint sets in the model is enlarged with the same ratio based on that in practice and the number of blocks in each model is maintained around 3.0×10^3. The exact number of rock blocks in the six models is shown in Table 1. Although such a simplification will reduce the reliability of the simulation results in certain aspects, e.g., the volumetric swelling of collapsed rock mass, it should have no decisive impact on the results of the slope instability, the main purpose of the simulation. Because both joint sets have good persistence in practice, the two joint sets are set to penetrate the models. Moreover, the hanging-wall ore-body is divided into three sections in the models, with the top section representing the actual induced caving subarea and the middle and bottom sections representing the actual sublevel caving subarea.

The numerical method used to do the simulations is the DDA method. It is an implicit method with good convergence to compute the static and dynamic behaviors of discrete systems of deformable blocks [23]. This method has been successfully applied to solve many rock mass dynamics problems [24]. In the DDA, each block can be of any shape and takes six variables, namely, $D_i = \left(u_0 \;\; v_0 \;\; r_0 \;\; \varepsilon_x \;\; \varepsilon_y \;\; \gamma_{xy}\right)^{\mathrm{T}}$, where the former three are for block displacements and the later three for block strains. The displacement increment in each time step at any point in the block is $(uv)^{\mathrm{T}} = \mathrm{T}_i D_i$, where

$$T_i = \begin{pmatrix} 1 & 0 & -(y-y_0) & (x-x_0) & 0 & (y-y_0)/2 \\ 0 & 1 & (x-x_0) & 0 & (y-y_0) & (x-x_0)/2 \end{pmatrix}. \tag{1}$$

Individual blocks are connected and form a block system by contacts between blocks and constraints on single blocks.

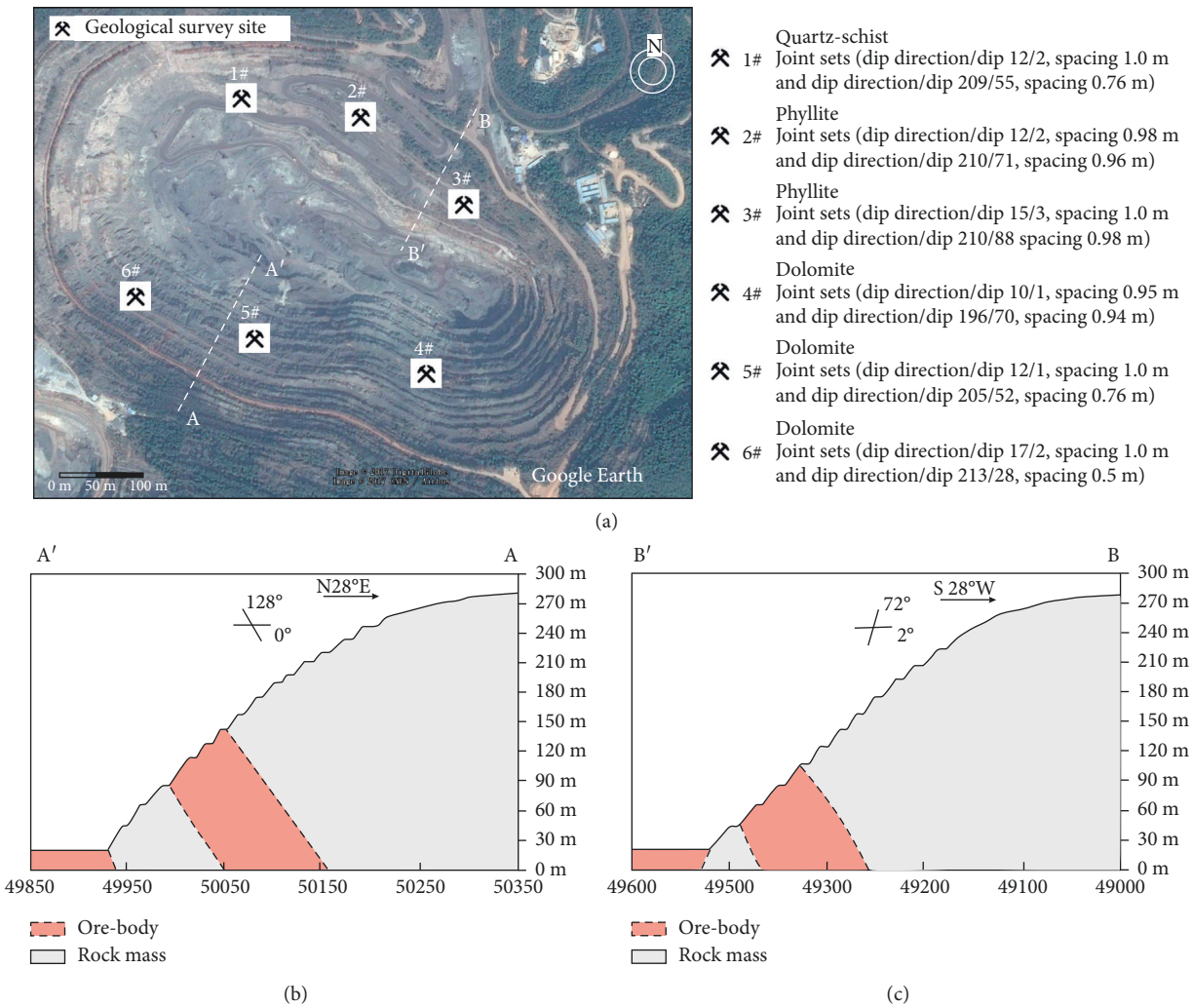

Figure 5: Distribution of geological survey sites and sectional views of the south and north slopes. (a) Geological survey sites. (b) South slope. (c) North slope.

Assuming there are n blocks in the defined block system, the simultaneous equilibrium equations have the following form:

$$\begin{pmatrix} \mathbf{K}_{11} & \mathbf{K}_{12} & \mathbf{K}_{13} & \cdots & \mathbf{K}_{1n} \\ \mathbf{K}_{21} & \mathbf{K}_{22} & \mathbf{K}_{23} & \cdots & \mathbf{K}_{2n} \\ \mathbf{K}_{31} & \mathbf{K}_{32} & \mathbf{K}_{33} & \cdots & \mathbf{K}_{3n} \\ \vdots & \vdots & \vdots & \ddots & \vdots \\ \mathbf{K}_{n1} & \mathbf{K}_{n2} & \mathbf{K}_{n3} & \cdots & \mathbf{K}_{nn} \end{pmatrix} \begin{Bmatrix} \mathbf{D}_1 \\ \mathbf{D}_2 \\ \mathbf{D}_3 \\ \vdots \\ \mathbf{D}_n \end{Bmatrix} = \begin{Bmatrix} \mathbf{F}_1 \\ \mathbf{F}_2 \\ \mathbf{F}_3 \\ \vdots \\ \mathbf{F}_n \end{Bmatrix}, \quad (2)$$

where $\mathbf{F}_i$ is the loading on block i distributed to the six deformation variables. Submatrix $\mathbf{K}_{ii}$ depends on the material properties of block i and $\mathbf{K}_{ij}$ where $i \neq j$ is defined by the contacts between block i and block j.

The physical and numerical control parameters used in the DDA simulations in this section are listed in Table 2. Generally, the physical parameters are based on some laboratory tests, such as density test, deformation test, compressive strength test, tensile strength test, and shear test, etc. It is assumed that strength degradation will take place to a joint [25], so the cohesion, tensile strength, and the friction angle values of the joint are reduced after failure, as shown in Table 2. The numerical control parameters are determined based on extensive trial simulations to achieve high computational efficiency with a small number of open-close iterations in each time step. A good review of the open-close iteration in the DDA to treat contact between blocks with the penalty method can be found in [26].

4.2. Excavation Time and Sequence. Using DDA static calculation, the initial stress equilibrium state of the model is obtained by applying gravity force to the blocks in the model. Thereafter, the excavation of the hanging-wall ore-body is executed, and the calculation turns to dynamic. Figure 7 shows the Y-direction stress evolution curves at measurement point MP1 (Figure 6) in the J1~J6 models. It is shown that the six models reach initial stress equilibrium at $t = 20$ s after approximate 20,000 time steps of DDA calculation. To

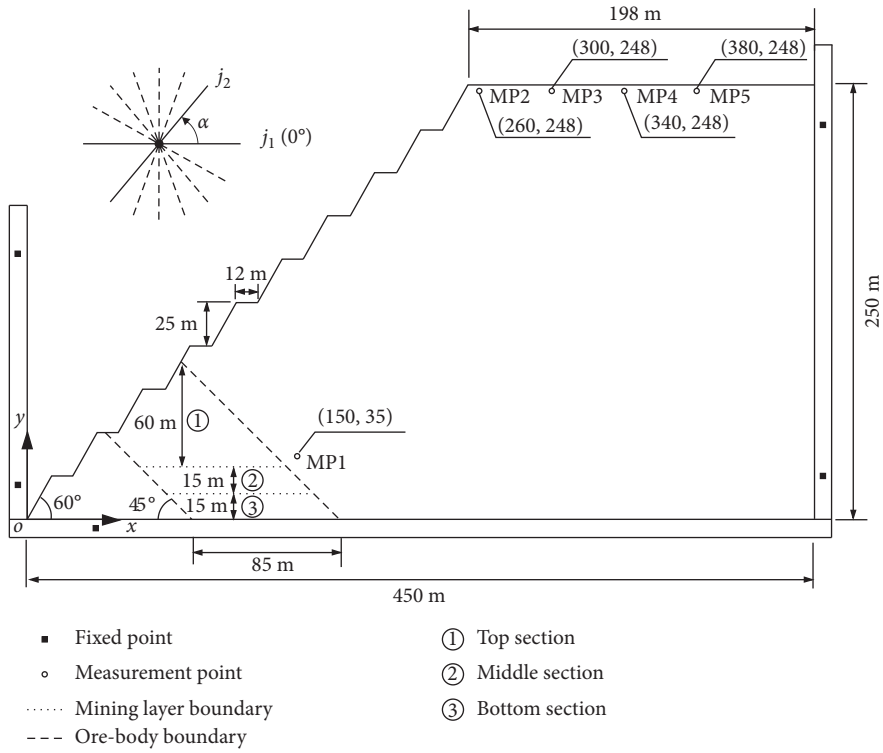

Figure 6: Geometric dimensions of the model and distributions of the measurement points (MPs).

Table 1: Rock joint and block number information in the six models.

Model index	Dip angle α of j_2 (degree)	Joint spacing of j_1, j_2 (m)	Block number
J1	50	5.0, 3.8	3116
J2	70	5.0, 4.7	3090
J3	90	5.0, 5.0	3077
J4	110	5.0, 4.7	3089
J5	130	5.0, 3.8	3099
J6	150	5.0, 2.5	3120

Table 2: Mechanical and numerical control parameters of the models.

	Parameter	Value
Physical parameters	Density	2780 kg/m^3
	Young's modulus	28 Gpa
	Poisson's ratio	0.25
	Joint cohesion (before/after failure)	0.22 MPa/0 MPa
	Joint tensile strength (before/after failure)	0.15 MPa/0 MPa
	Joint friction angle (before/after failure)	36°/30°
	Kinematic condition (before/after excavation)	Static/Dynamic
Numerical control parameters	Time-step (before/after excavation)	0.001 s/0.0001 s
	Displacement ratio (before/after excavation)	0.001/0.001
	Normal/shear spring stiffness	350 GPa/140 GPa

simulate actual mining operations, the hanging-wall orebody is excavated by two steps, with the first step to excavate the induced caving subarea and the second step to excavate the sublevel caving subarea. The second excavation is performed at the end of the slope instability caused by the first excavation, and the whole calculation finishes when the slope instability caused by the second excavation completes. Figure 8 takes the J4 model (0°/110°) as an example to show the horizontal displacement evolution curves of the four measurement points MP2–MP5 locating on the top surface of the slope. In the J4 model, the first excavation is executed at the 20,000 time step (t = 19.999100 s), whereas the second

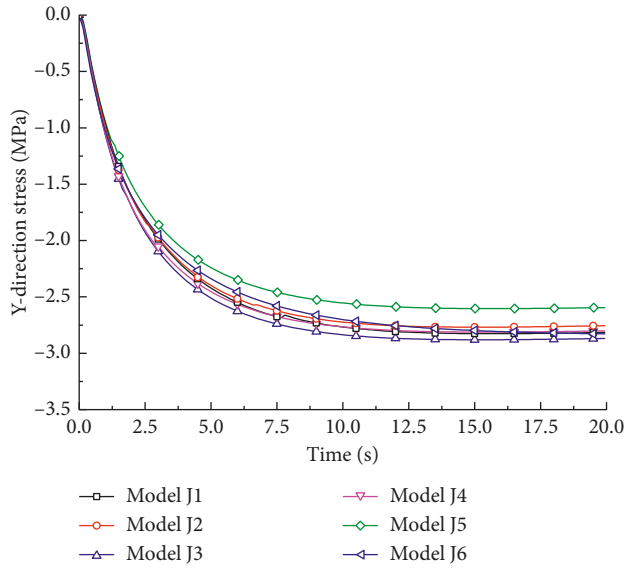

Figure 7: *Y*-direction stress curves of MP1 in J1~J6 model under the gravity force.

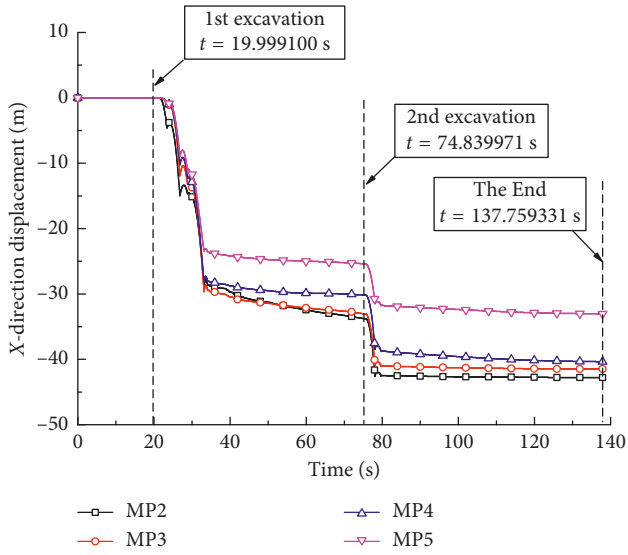

Figure 8: Horizontal displacement curves of MP2~MP5 in the J4 model.

excavation at the 570,000 time step (t = 74.839971 s). The whole calculation finishes at 1,200,000 time step (t = 137.759331 s). A series of trial calculation results show that the excavation time steps in the J4 model are also applicable to other five models. This group of simulations simplifies the mining excavation into two steps to save computer time with a focus to investigate the effect of the rock structure on the slope instability behavior in the proposed mining scheme of hanging-wall ore-body via the induced caving mining method. The impact of the mining sequence will be specifically studied in Section 5.

4.3. Analysis of Simulation Results. Figures 9(a)–9(e) show the slope states of the J1-J5 models at the 570,000 and 1,200,000 time step, which represent the slope instability morphologies after the first and second excavation, respectively. Figure 9(f) shows the slope states of the J6 model at the 100,000, 200,000, 570,000, and 1,200,000 time step, to demonstrate the whole failure process of the slope in more detail.

4.3.1. Slope Instability Mode. Figure 9 shows that different slope instability modes are observed under various rock mass structures. The instability modes can be categorized into sliding and toppling as predicted in Section 3. The sliding instability appears in the J1~J3 models, representing the conditions in the north slope, while the toppling instability appears in the J4~J6 models, representing the conditions in the south slope in practice, respectively.

In the J1~J3 models, joint set j_2 points to the toe of the slope. After the excavation of the hanging-wall ore-body, the resistance of the rock discontinuities becomes weaker than the sliding force of the rock under the slope free face; thus, the slope is destabilized and sliding failure takes place. In the J4~J6 models, j_2 points inwards the slope. Once the hanging-wall ore-body is excavated, the rock above in the slope will deform under the bending effect and topple into the mined-out area after the failure strength of the rock joints are reached. In the J1~J5 models, the deformation and movement of the adjacent failed strata seems continuous. Comparatively, in the J6 model, the rock falls off as sparse discrete clusters into the mined-out area. The entire failure process involves the separation, falling, rolling, and bouncing of the rock mass.

It can be found that joint set j_2 plays a dominant role in the slope failure to control the failure mode. A dip angle smaller than 90° is likely to induce sliding failures, while a value lager than 90° is likely to induce toppling failures. As for the J6 model, in addition to the gentle inclination of the j_2, the interlaced, long, and narrow rock blocks with sharp angles account for the special failure phenomena. The interlaced diamond-shaped blocks are beneficial for the slope to achieve stability during the toppling failure process.

4.3.2. Risk Assessment in Open-Pit Mining. Using the mined-out area generated by the planned mining of the hanging-wall ore-body to absorb the collapsed slope rock mass is the core idea of the proposed mining scheme. The above DDA simulation results show that whether the collapsed rock will endanger normal open-pit mining is closely related to the slope rock mass structure. Figure 10 shows the final profiles of collapsed slopes for the J1~J6 models.

As for the J1~J3 models, Figure 10 shows that in the J1 model, part of the collapsed blocks rush to the bottom of the open pit, threatening the open-pit mining below, whereas, the profiles of the collapsed slopes in the J2 and J3 models are obviously lower than the original slope profiles, which indicates that the mined-out area in these two models can sufficiently absorb the collapsed rock; thus, the open-pit mining is safe. From these three models, it is concluded that a gentle inclination of the predominant joint set indicates that the collapsed rock mass is more likely to slide downwards to the bottom of the open pit to threaten open-pit mining.

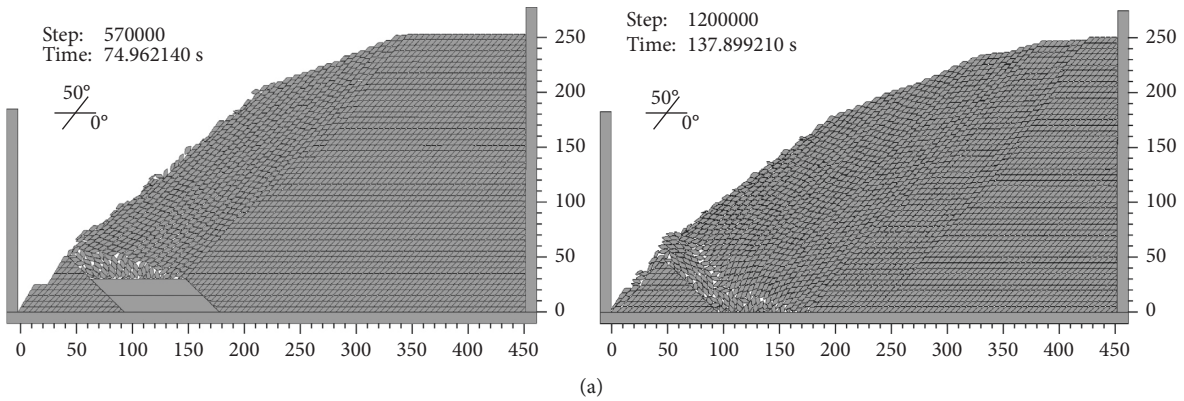

(a)

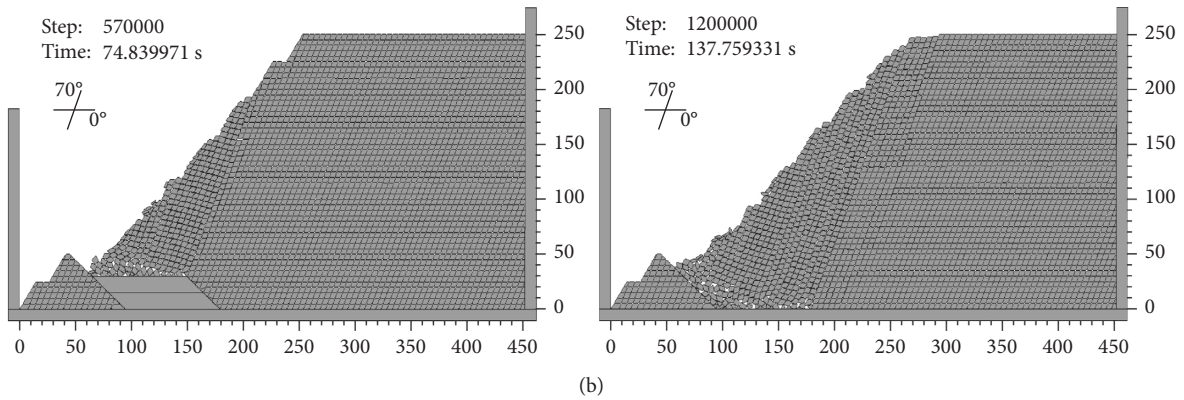

(b)

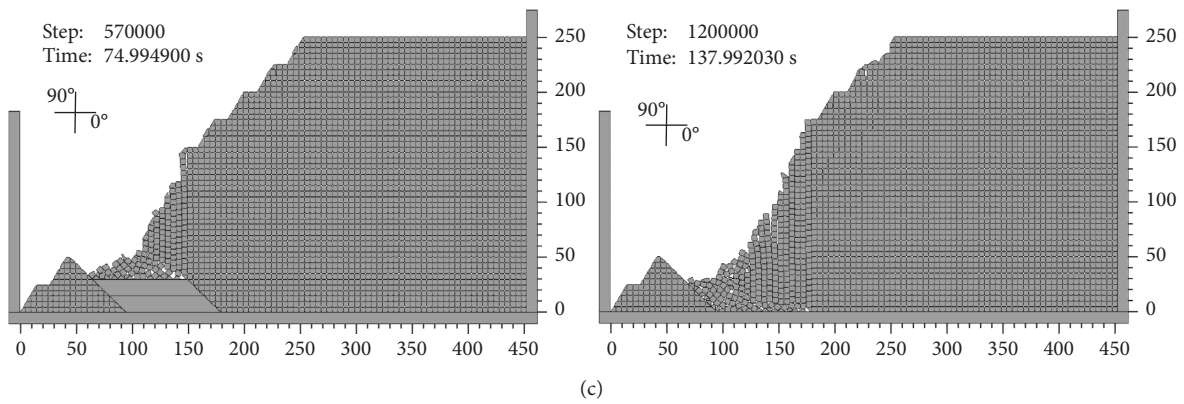

(c)

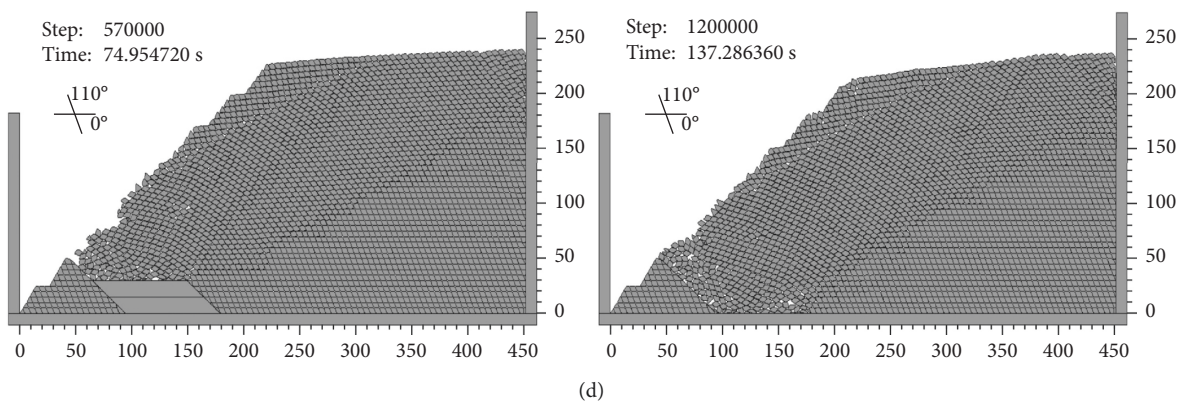

(d)

Figure 9: Continued.

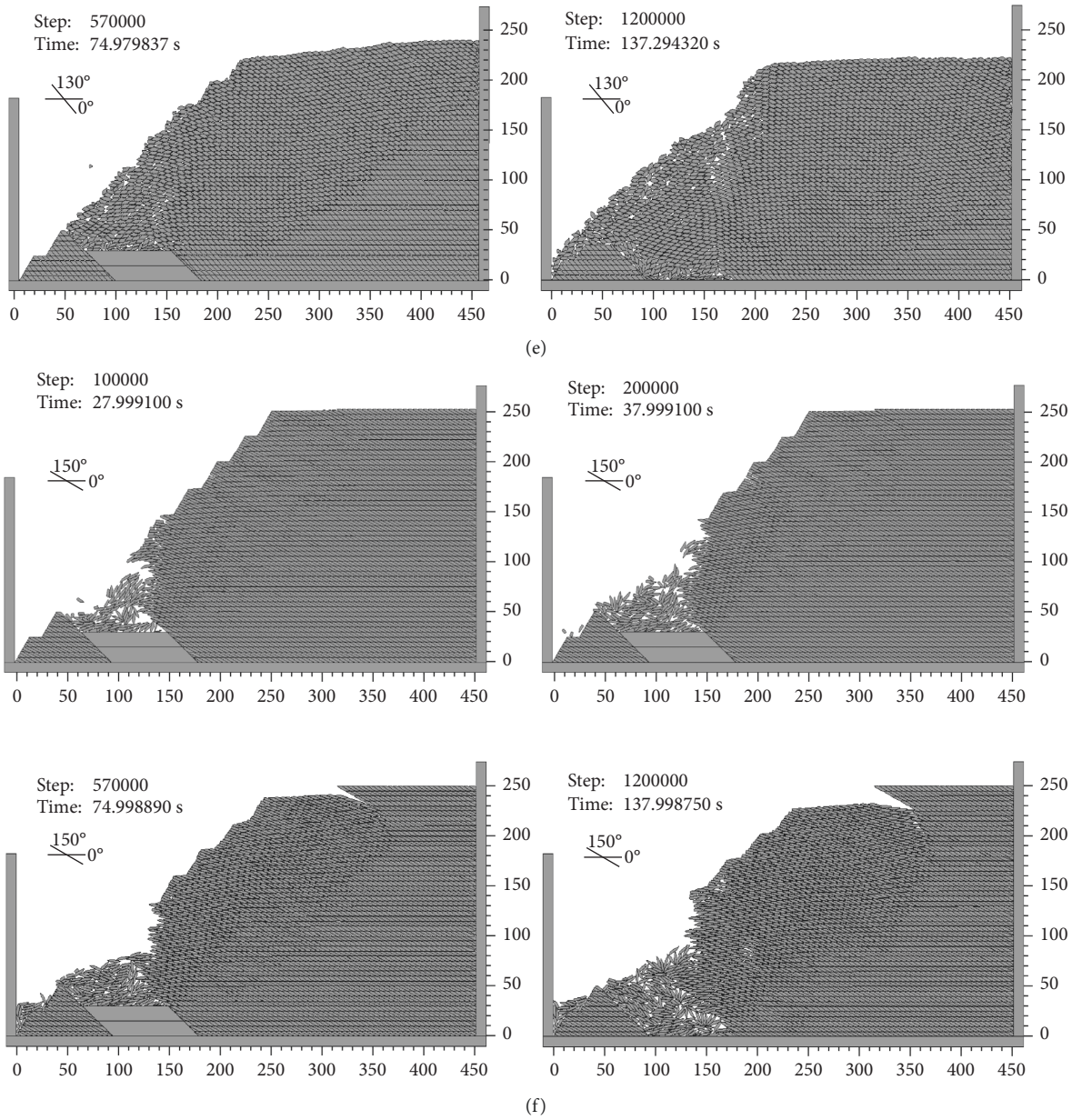

Figure 9: Slope instability in hanging-wall ore-body mining via induced caving for models J1~J6. (a) Model J1. (b) Model J2. (d) Model J4. (e) Model J5. (f) Model J6.

For the J4~J6 models, a large number of collapsed blocks rush to the bottom of the open pit in the J5 model. It is worth noting that although a bulgy slope profile is formed in the J5 model after the first excavation, there are no blocks rushing to the bottom of the open pit until the second excavation, as shown Figure 9(e). It shows that as the mining of the hanging-wall ore-body proceeds, the risk may increase. In the J4 model, although no bulk rock blocks rush towards the bottom of the open pit, the profile of the final collapsed slope has a high degree of coincidence with the original slope profile before hanging-wall ore-body mining. The above conclusion from the J5 model indicates that there exist potential threats to the open-pit mining if further mining of the hanging-wall ore-body in model J4 is carried out. The profile of the collapsed slope in the J6 model is not as full as that of the J5 and J4 models; however, individual collapsed blocks bounced out to the bottom of the open pit, which also poses a threat to the open-pit mining. This is because the long and narrow blocks in model J6 fall off sporadically and get quite large kinematic energy after the hanging-wall ore-body is excavated.

Additional measures, such as retaining dams and arresting barriers, can be used to bar rolling rocks. However, such practice is generally passive and unreliable in the case of a large amount of rolling stones. Therefore, the present study proposes to eliminate the possible threat of the collapsed rock mass to the open-pit mining.

As indicated by the simulation results of the J1~J6 models, the mode of slope instability due to induced caving of the hanging-wall ore-body, as well as the possible threat

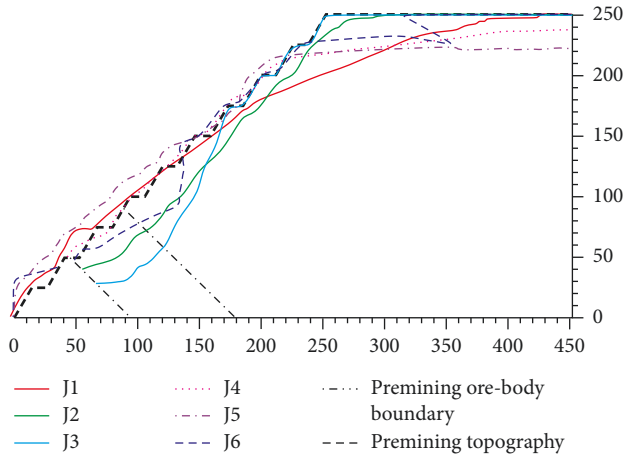

Figure 10: Profiles of the collapsed slopes for the J1~J6 models.

of the inner-slope mining to the open-pit mining, has a closely relationship with the slope rock structure. For a given geological condition of hanging-wall ore-body, the feasibility of the application of the proposed mining scheme can be expected to be achieved by adjusting the exact mining plan, e.g., optimizing the mining sequence, as investigated below in Section 5.

5. Influence of Mining Sequence

For the Hainan Iron Mine, mining the hanging-wall ore-body under the south slope during the transition stage is more suitable because the open-pit haulage road is situated on the north slope. Figure 11 shows the production condition of the open pit. According to the previous numerical simulation results, using the induced caving mining method to extract hanging-wall ore-body under the south slope will trigger slope topping failure. Topping failure is highly likely to cause massive slope destruction; therefore, numerous collapsed rock blocks that rush from the slope to the bottom of the open pit may harm normal surface mining (as illustrated by Model J5). Here, the mining of hanging-wall ore-body under the south slope is taken as an example, and four simulation scenarios with different mining sequence are designed to explore the effect of mining sequence on the development of slope instability and the mining safety, so as to determine a highly reliable mining sequence to guide the actual mining design.

5.1. Model Establishment. The layout of the rock structure is provided in Figure 5(a). The ore-body under the slope has two joint sets, one of which is approximately horizontal and the other is approximately vertical, both with a spacing around 1.0 m. By combining the strength, mode of occurrence, depth, and location of hanging-wall ore-body with the actual mining experience, the initial mining level (undercut level) is tentatively set at an elevation of 60 m, with the second mining level at 45 m and the third mining level at 30 m. Figure 12(a) shows the layout of the stope structure on the A–A′ section (Figure 5(a)). Figures 12(b) and 12(c) illustrate the model geometry and the corresponding DDA model, respectively. Different from the above-mentioned six models in Section 4, the present model not only sets the undercut level but also partitions the 2~4 mining levels into independent blocks. Excavation of each independent block in the 2~4 mining levels represents the actual mining of a production drift; thus, different mining sequences may be set within a mining layer. Table 3 lists the physical parameters of the ore-body. The physical parameters of the rock and the DDA numerical control parameters are the same as that in Table 2. The joint sets of the ore-body and rock mass in the model are also set as penetrating joints, and the joint spacing of the ore-body and rock is both increased by 5 times to 5.0 m, producing 3,072 blocks eventually in the DDA model.

5.2. Mining Sequence. Similar to the previous simulation examples, solving the initial stress equilibrium of the model is necessary prior to excavating hanging-wall ore-body. Figure 13 plots the evolution curve of the stresses of measurement point MP1 (Figure 12(b)). It is shown that the model reaches the initial stress equilibrium after the 20,000 time step (t = 19.86700 s); then, the undercut level is excavated. Thereafter, the roof under the combined action of the stress redistribution and the gravity cave into the undercut, and the slope suffers topping instability simultaneously. However, the failure and movement of the slope rock mass are limited due to the supporting role of the caved ore, as shown in Figure 14(a). Then, the caved ore is removed, representing the ore-drawing operation in practice. The removal of the caved ore is accompanied by a further massive topping instability of the slope, as shown in Figure 14(b). At this time, a bulgy loose slope is formed. However, no bulk rock blocks rush in the bottom of the open pit, which indicates that setting the undercut level at 60 m is reasonable.

Based on the results of the J5 model above, the risk of bulk rock rushing downwards to the open pit from the slope may increase with the further mining progress. Therefore, to seek for the following optimally safe mining plan, four scenarios with different mining sequences for the 2~4 mining levels in the model, as shown in Figure 15, are considered. Scenario 1~3 starts from the outside slope inwards, the inside slope outwards, and center to both sides, respectively. Scenario 4 has similar mining sequence with scenario 3; however, a safety ore-pillar of a certain size is reserved near the hanging-wall of the ore-body, and it is excavated in the end. The size of the safety ore-pillar is not designed based on its stability analysis but on the assumption that it does not fail during the mining.

5.3. Analysis of the Simulation Results. Figure 16 shows the numerical simulation results of the slope failure conditions for the four mining scenarios. Slope instability occurs in scenarios 1~3, with bulk rock rushing to the bottom of the open pit from the slope, in which scenario 2 is the most serious (rushing of bulk rock to the bottom of the open pit takes place the earliest as well), followed by scenario 1,

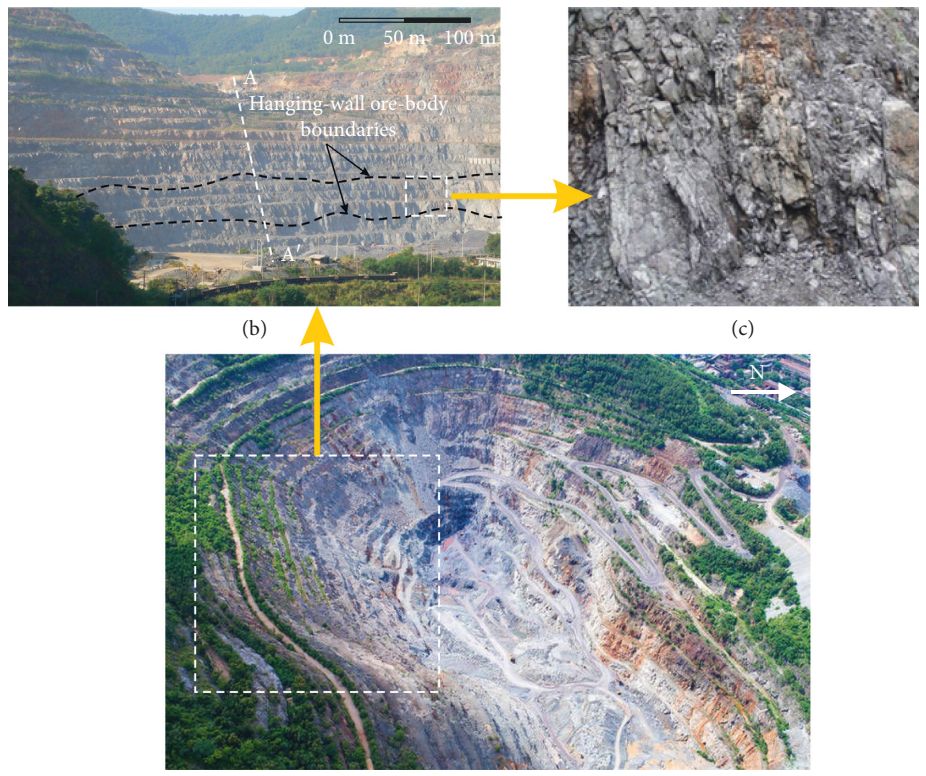

Figure 11: Production condition of the open pit. (a) Aerial view, (b) south slope with the sectional view shown in Figure 4(b), and (c) broken outcrop.

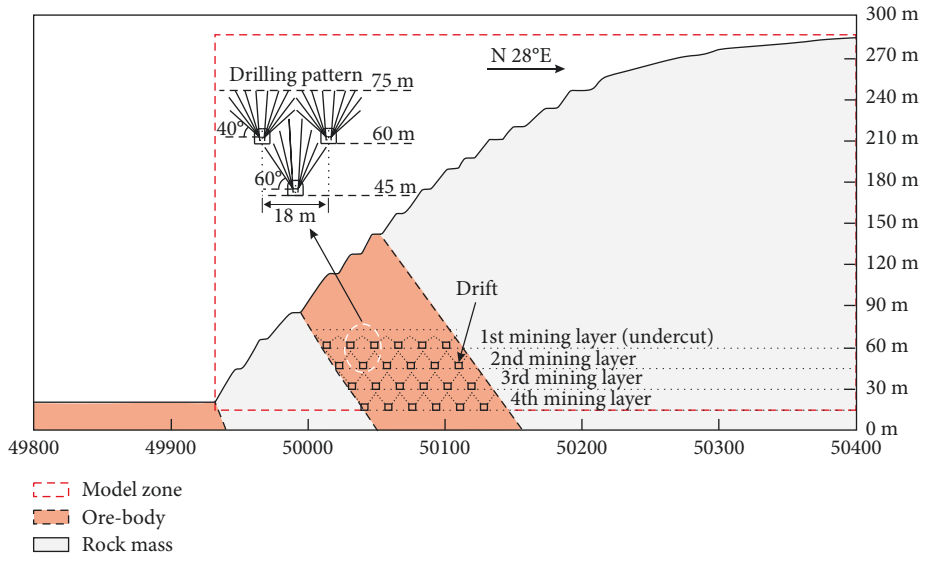

(a)

Figure 12: Continued.

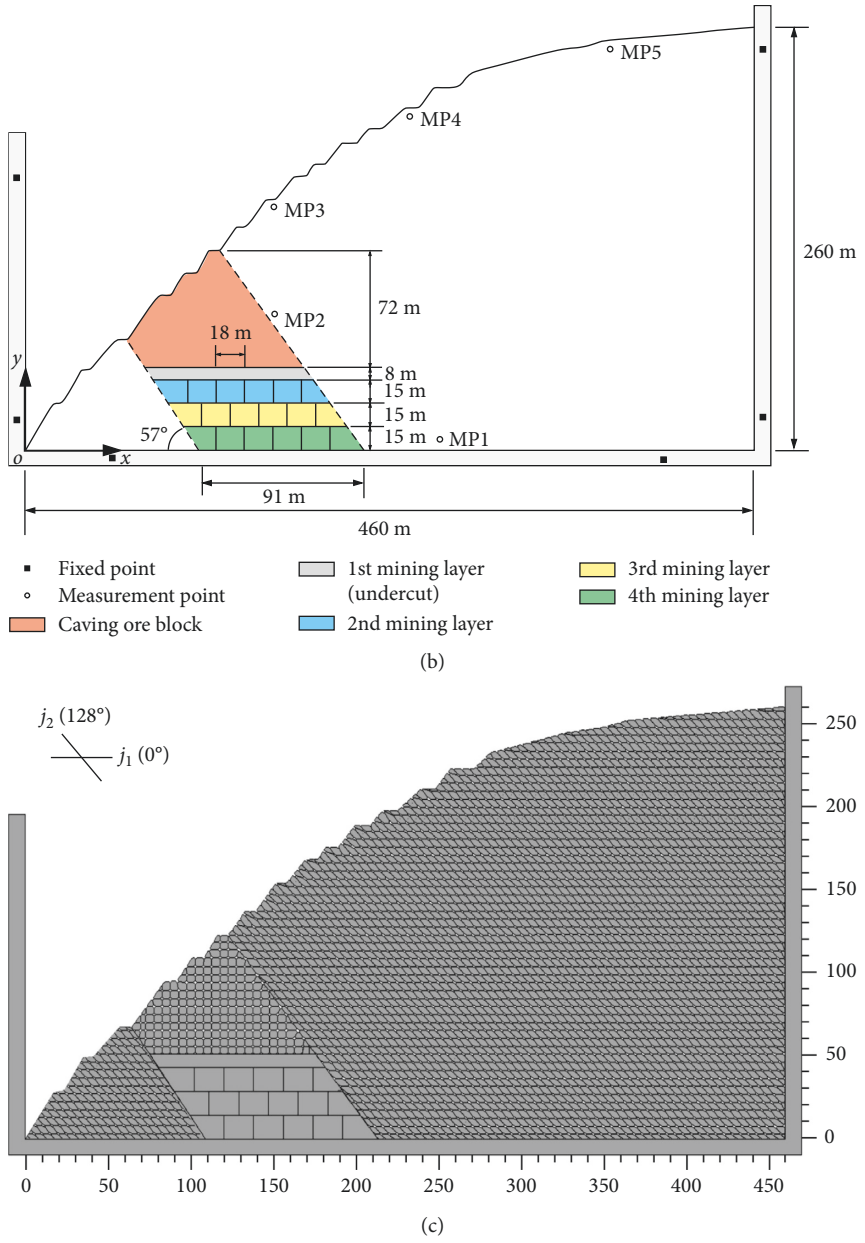

Figure 12: Stope layout and the DDA Model. (a) Layout of the stope structure on the A–A′ section. (b) Model geometry and distribution of measurement points. (c) DDA model.

Table 3: Physical parameters of the ore-body.

Parameter	Value
Density	4150 kg/m^3
Young's modulus	25 Gpa
Poisson's ratio	0.27
Joint cohesion (before/after failure)	0.18 MPa/0 MPa
Joint tensile strength (before/after failure)	0.1 MPa/0 MPa
Joint friction angle (before/after failure)	32°/25°

whereas scenario 3 is obviously alleviated. In comparison with scenarios 1 and 2, the mining sequence from the center to both sides in scenario 3 effectively reduces the risk of massive bulk rock rushing to the bottom of the open pit, thereby improving the mining safety to a large extent. However, more satisfactorily, no rushing of rock blocks to the bottom of the open pit occurs throughout the mining process in scenario 4. As compared with scenario 3, the spread of slope failure is effectively reduced due to reservation of the ore-pillar. Moreover, it can be found that with the help of a reasonable mining sequence, collapsed slope rock mass could be induced to rush to the mined-out area, such that the profile of the collapsed slope can become concaved, thereby greatly guaranteeing the safety of open-pit mining.

The above results indicate that when using the induced caving mining method to extract hanging-wall ore-body during the transition from open pit to underground

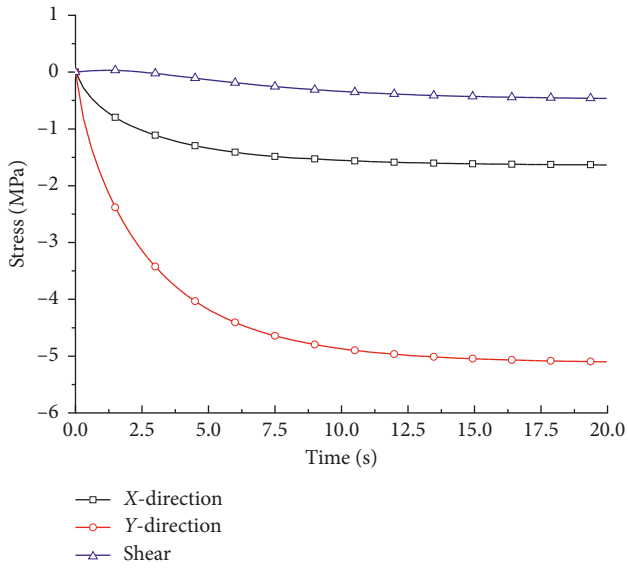

Figure 13: Stress curves of measurement point MP1 under the gravity force.

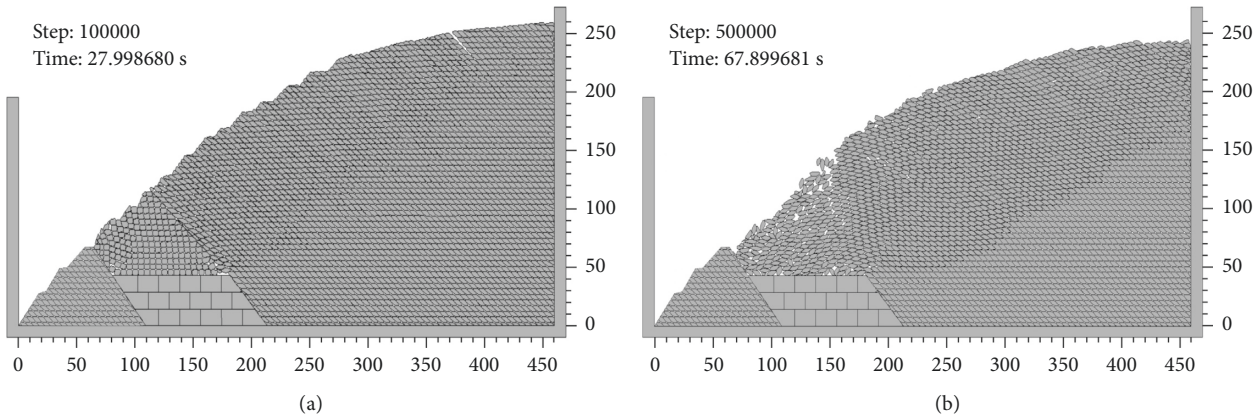

Figure 14: Slope instability after undercutting (a) and removing the caved ore (b).

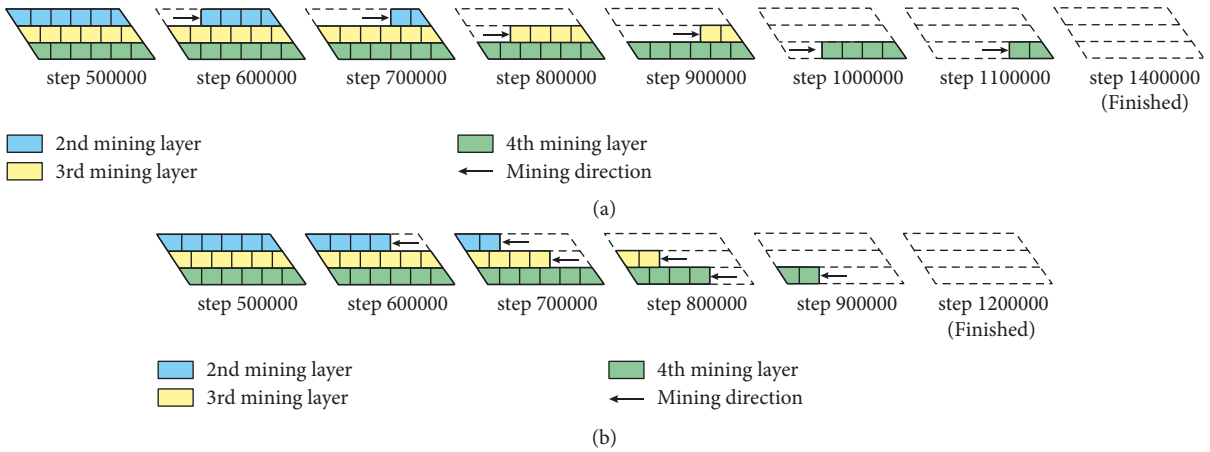

Figure 15: Continued.

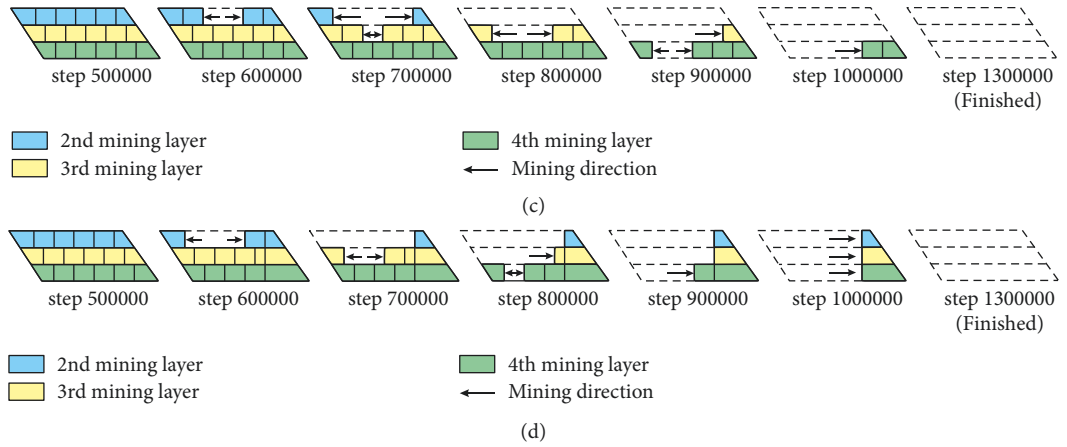

Figure 15: Four mining scenarios with different mining sequences. (a) Scenario 1, (b) Scenario 2, (c) Scenario 3, (d) Scenario 4.

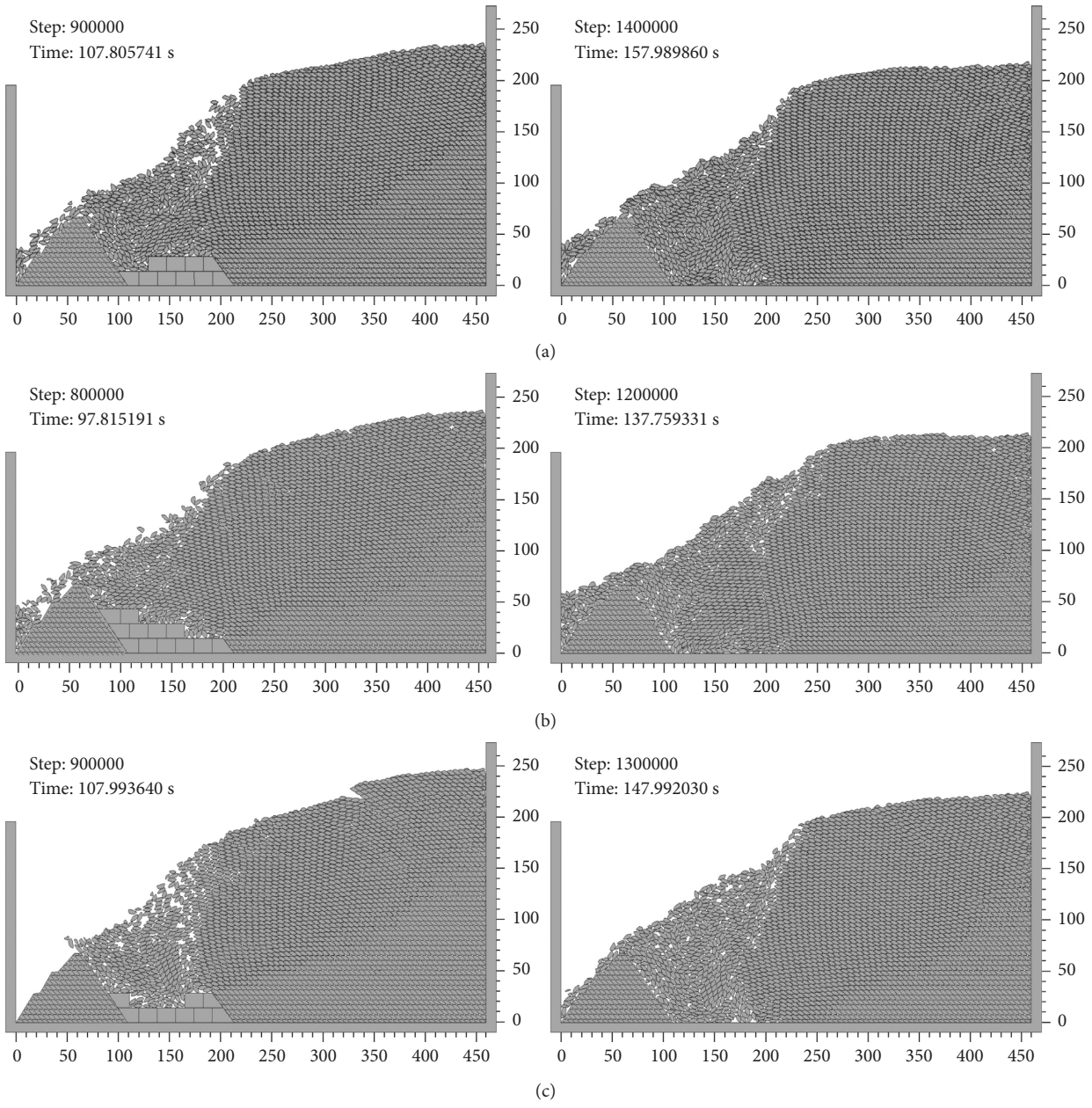

Figure 16: Continued.

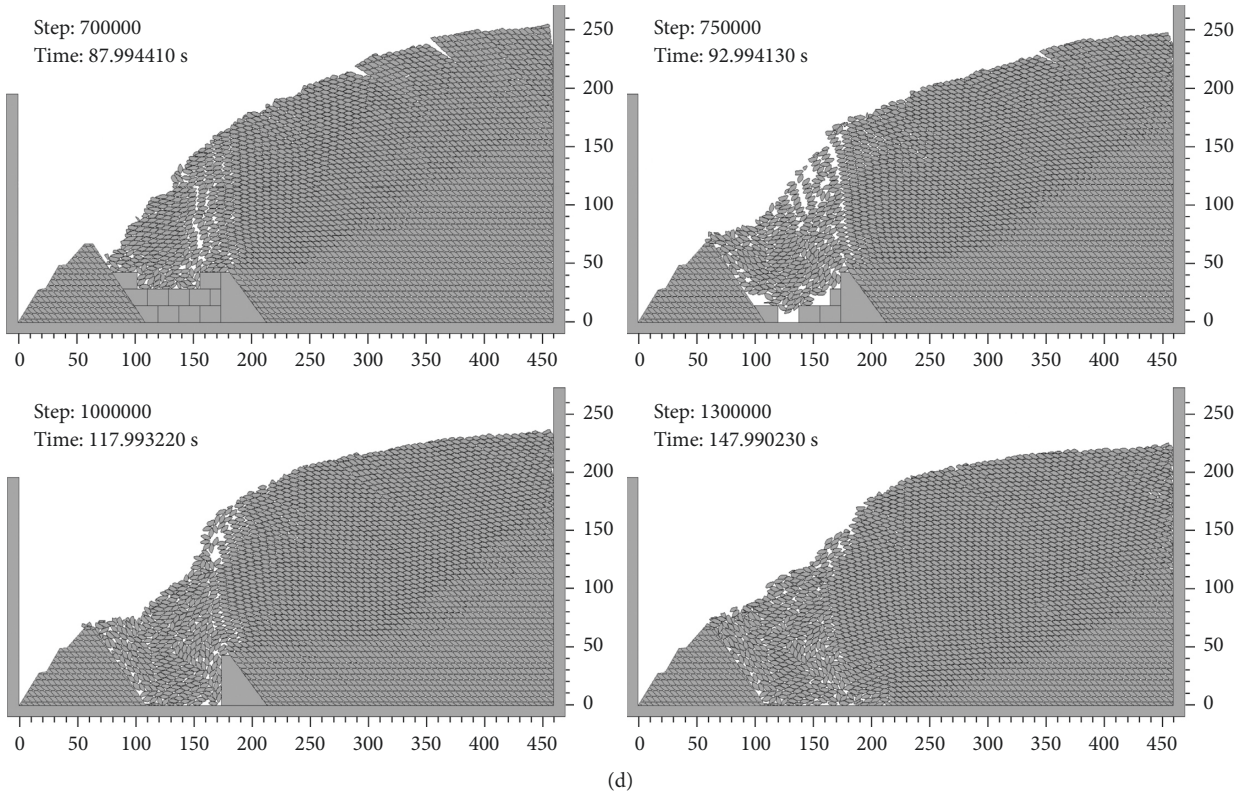

(d)

Figure 16: Slope instability of the four mining scenarios. (a) Scenario 1. (b) Scenario 2. (c) Scenario 3. (d) Scenario 4.

mining, the risk of collapsed slope rock mass rushing to the bottom of the open pit to threaten the open-pit mining is capable to be eliminated by optimizing the mining plan, including adjusting of the mining sequence, even under the condition of topping-induced massive slope instability.

6. Conclusions

In this study, a mining scheme for hanging-wall ore-body via the induced caving mining method during the transition from open pit to underground mining is proposed. The numerical simulation in this study proves the feasibility of the proposed mining scheme and explored its mechanism and some critical impacting factors including the rock structure and the mining sequence.

The numerical simulation results show that the mode of slope instability triggered by the induced caving mining of the hanging-wall ore-body is closely correlated with the rock mass joint orientations of the slope. When the predominant joint set enables sliding instability of the slope, a more gentle inclination of the predominant joint set means a higher possibility of the rushing out of the collapsed rock mass to the bottom of the open pit as a threat. Comparatively, when the predominant joint set hints topping instability of the slope, the relationship between the inclination of the predominant joint set and the threat of the collapsed slope rock to the open-pit mining becomes further complicated because certain joint set interactions turn to against the failure of the slope. Moreover, the mining sequence of hanging-wall ore-body has a significant impact on the development of slope instability and its threat to the open-pit mining. A reasonable mining sequence of the hanging-wall ore-body can help to effectively eliminate the threat that slope instability poses to the normal open-pit mining. These conclusions are instructive to the mining design of actual engineering.

Generally, the proposed mining scheme for hanging-wall ore-body via induced caving breaks the traditional concept that the slope must remain stable during the transition stage, which avoids the mutual restriction of hanging-wall ore-body mining and normal open-pit mining, and helps to realize smooth transition for the ore output during the transition from open-pit to underground mining. This mining scheme is hopefully to be applied and validated in practical mining engineering in the future.

Data Availability

The data used to support the findings of this study are available from the corresponding author upon request.

Conflicts of Interest

The authors declare that they have no conflicts of interest.

Acknowledgments

The authors would like to thank the financial support provided by the National Key Research and Development Program of China (grant no. 2016YFC0801601), the

National Natural Science Foundation of China (grant no. 51534003), the Open Projects of State Key Laboratory of Coal Resources and Safe Mining of CUMT, China (grant no. SKLCRSM16KF08).

References

[1] K. Liu, W. Zhu, Q. Wang et al., "Mining method selection and optimization for hanging-wall ore-body at Yanqianshan Iron Mine, China," *Geotechnical and Geological Engineering*, vol. 35, no. 1, pp. 1–17, 2016.

[2] N. X. Xu, J. Y. Zhang, H. Tian, G. Mei, and Q. Ge, "Discrete element modeling of strata and surface movement induced by mining under open-pit final slope," *International Journal of Rock Mechanics and Mining Sciences*, vol. 88, pp. 61–76, 2016.

[3] E. Bakhtavar, "Transition from open-pit to underground in the case of Chah-Gaz iron ore combined mining," *Journal of Mining Science*, vol. 49, no. 6, pp. 955–966, 2013.

[4] S. Opoku and C. Musingwini, "Stochastic modelling of the open pit to underground transition interface for gold mines," *International Journal of Surface Mining Reclamation and Environment*, vol. 27, no. 6, pp. 407–424, 2013.

[5] Y. Zhao, T. Yang, M. Bohnhoff et al., "Study of the rock mass failure process and mechanisms during the transformation from open-pit to underground mining based on microseismic monitoring," *Rock Mechanics & Rock Engineering*, vol. 51, no. 5, pp. 1473–1493, 2018.

[6] Y. Zhao, S. Wang, Z. Zou et al., "Instability characteristics of the cracked roof rock beam under shallow mining conditions," *International Journal of Mining Science and Technology*, vol. 28, no. 3, pp. 437–444, 2018.

[7] N. Lin, T. Sasaoka, H. Shimada, A. Hamanaka, and K. Matsuia, "Numerical analysis of interaction effects in double extra-thick coal seams mining," *Procedia Earth Planet Sci*, vol. 6, pp. 343–349, 2013.

[8] X. Li, D. Li, Z. Liu, G. Zhao, and W. Wang, "Determination of the minimum thickness of crown pillar for safe exploitation of a subsea gold mine based on numerical modelling," *International Journal of Rock Mechanics and Mining Sciences*, vol. 57, pp. 42–56, 2013.

[9] D. P. Kanungo, A. Pain, and S. Sharma, "Finite element modeling approach to assess the stability of debris and rock slopes: a case study from the Indian Himalayas," *Natural Hazards*, vol. 69, no. 1, pp. 1–24, 2013.

[10] J. P. Yang, W. Z. Chen, Y. H. Dai et al., "Numerical determination of elastic compliance tensor of fractured rock masses by finite element modeling," *International Journal of Rock Mechanics and Mining Sciences*, vol. 70, pp. 474–482, 2014.

[11] M. C. Jaime, Y. Zhou, J. S. Lin et al., "Finite element modeling of rock cutting and its fragmentation process," *International Journal of Rock Mechanics & Mining Sciences*, vol. 80, no. 4, pp. 137–146, 2015.

[12] C. Müller, T. Frühwirt, D. Haase et al., "Modeling deformation and damage of rock salt using the discrete element method," *International Journal of Rock Mechanics and Mining Sciences*, vol. 103, pp. 230–241, 2018.

[13] K. T. Chen and J. H. Wu, "Simulating the failure process of the Xinmo landslide using discontinuous deformation analysis," *Engineering Geology*, vol. 239, pp. 269–281, 2018.

[14] Y. Ju, H. Sun, M. Xing et al., "Numerical analysis of the failure process of soil–rock mixtures through computed tomography and PFC3D models," *International Journal of Coal Science and Technology*, vol. 6, no. 2, pp. 126–141, 2018.

[15] Y. H. Hatzor, X. T. Feng, S. Li et al., "Tunnel reinforcement in columnar jointed basalts: the role of rock mass anisotropy," *Tunnelling and Underground Space Technology Incorporating Trenchless Technology Research*, vol. 46, pp. 1–11, 2015.

[16] P. Hamdi, D. Stead, D. Elmo et al., "Use of an integrated finite/discrete element method-discrete fracture network approach to characterize surface subsidence associated with sub-level caving," *International Journal of Rock Mechanics and Mining Sciences*, vol. 103, pp. 55–67, 2018.

[17] A. Vyazmensky, D. Stead, D. Elmo, and A. Moss, "Numerical analysis of block caving induced instability in large open pit slopes: a finite element/discrete element approach," *Rock Mech Rock Eng*, vol. 43, no. 1, pp. 21–39, 2010.

[18] Y. J. Ning, X. M. An, and G. W. Ma, "Footwall slope stability analysis with the numerical manifold method," *International Journal of Rock Mechanics and Mining Sciences*, vol. 48, no. 6, pp. 964–975, 2011.

[19] D. H. Laubscher, *Block Caving Manual, Prepared for International Caving Study*, JKMRC and Itasca Consulting Group, Inc., Brisbane, Australia, 2000.

[20] L. Quiñones, C. Lagos, F. Ortiz, E. Farías, L. Toro, and D. Villegas, "Undercut advance direction management at the North 3rd Panel, Rio Blanco Mine, División Andina Codelco Chile," in *Proceedings of the Third International Symposium on Block and Sublevel Caving*, Santiago, Chile, June 2014.

[21] R. E. Goodman and D. S. Kieffer, "Behavior of rock in slopes," *Journal of Geotechnical and Geoenvironmental Engineering*, vol. 126, no. 8, pp. 675–684, 2000.

[22] G. Yagoda Biran and Y. H. Hatzor, "A new failure mode chart for toppling and sliding with consideration of earthquake inertia force," *International Journal of Rock Mechanics and Mining Sciences*, vol. 64, pp. 122–131, 2013.

[23] G. H. Shi, "Discontinuous deformation analysis: a new numerical model for the statics and dynamics of deformable block structures," *Engineering Computations*, vol. 9, no. 2, pp. 157–168, 1992.

[24] Y. Ning, Z. Yang, B. Wei et al., "Advances in two-dimensional discontinuous deformation analysis for rock-mass dynamics," *International Journal of Geomechanics*, vol. 17, no. 5, article E6016001, 2016.

[25] Y. Ning, J. Yang, X. An et al., "Modelling rock fracturing and blast-induced rock mass failure via advanced discretisation within the discontinuous deformation analysis framework," *Computers and Geotechnics*, vol. 38, no. 1, pp. 40–49, 2011.

[26] H. Bao, Z. Zhao, and Q. Tian, "On the Implementation of augmented Lagrangian method in the two—dimensional discontinuous deformation analysis," *International Journal for Numerical and Analytical Methods in Geomechanics*, vol. 38, no. 6, pp. 551–571, 2014.